PAPER

Sn-doped CdTe as promising intermediate-band photovoltaic material

IOP Publishing Journal of Physics D: Applied Physics
J. Phys. D: Appl. Phys. **50** (2017) 035501 (8pp) doi:10.1088/1361-6463/50/3/035501

Sn-doped CdTe as promising intermediate-band photovoltaic material

Mauricio A Flores[1,2], Eduardo Menéndez-Proupin[3], Walter Orellana[4] and Juan L Peña[5]

[1] Facultad de Ciencias, Pontificia Universidad de Católica de Valparaíso, Casilla 4950, Valparaíso, Chile
[2] Facultad de Ingeniería y Tecnología, Universidad San Sebastián, Bellavista 7, Santiago 8420524, Chile
[3] Departamento de Física, Facultad de Ciencias, Universidad de Chile, Las Palmeras 3425, 780-0003 Ñuñoa, Santiago, Chile
[4] Departamento de Ciencias Físicas, Universidad Andres Bello, Sazié 2212, 037-0136 Santiago, Chile
[5] Applied Physics Department, CINVESTAV-IPN, Apdo. Postal 73, Mérida, Yucatán, 97310, Mexico

E-mail: mauricio.flores@ug.uchile.cl

Received 25 September 2016, revised 1 November 2016
Accepted for publication 8 November 2016
Published 9 December 2016

Abstract

The formation energies, charge transition levels and quasiparticle defect states of several tin-related impurities are investigated within the DFT + *GW* formalism. The optical spectrum obtained from the solution of the Bethe–Salpeter equation shows that the absorption strongly increases in the sub-bandgap region after doping, suggesting a two-step photoexcitation process that facilitates transitions from photons with insufficient energy to cause direct transitions from the valence to the conduction band via an intermediate-band. We propose Sn-doped CdTe as a promising candidate for the development of high-efficiency solar cells, which could potentially overcome the Shockley–Queisser limit.

Keywords: CdTe, photovoltaics, intermediate-band, solar cells

(Some figures may appear in colour only in the online journal)

1. Introduction

In a traditional semiconductor photovoltaic cell electrons are excited from the valence band (VB) to the conduction band (CB). The efficiency of a solar cell is closely related to the generation of photoinduced electron-hole pairs and their recombination before being extracted. Moreover, a large amount of the converted photon energy is lost due to the rapid thermalization of carriers with energies higher than those of the semiconductor band gap. Hence, the limiting conversion efficiency for a single-junction solar cell is given by the assumption of extracting completely thermalized carriers from a single band gap absorber, namely, the Shockley–Queisser (SQ) limit [1].

Several ways to exceed the SQ limit have been explored by several researchers. Multi-junction solar cells (MJ-SC) based on the spectral splitting principle have been devised, achieving conversion efficiencies over 40% [2, 3]. However, due to their high manufacturing cost, they are only used in concentrator systems and space applications. Another concept for high conversion efficiency is the idea of a hot-carrier solar cell (HC-SC) [4, 5], in which photo-generated carriers of high energies are extracted before they are completely thermalized [4, 5], but are not yet competitive to MJ-SCs. A third approach is to increase the photocurrent via two-step photoexcitation by using an isolated intermediate-band (IB) as a stepping stone [6, 7]. The latter approach is the subject of the present work.

Inserting a partially filled IB into the forbidden band gap enables two additional transitions to the unoccupied bands (VB → IB and IB → CB), allowing the absorption of sub-bandgap photons [8–10]. This process yields enhancement of the photocurrent without degrading the open-circuit voltage. Additionally, it reduces the energy losses due to the thermal relaxation of the optically excited carriers [11]. Under illumination, the Fermi level splits into three quasi-Fermi levels, one each for both the VB and the CB, and one for the IB [7]; thereby, three absorption bands are capable of producing an electron-hole pair. This kind of solar cell could achieve efficiencies higher than those established by the SQ limit of 40.7% for single-junction solar cells under full concentration. The theoretical limiting efficiency for IBSCs is estimated to

be as high as 63.2% for a semiconductor with a band gap of 1.98 eV [7], comparable to the efficiency for optimized triple-junction solar cells [7, 12].

The quest for finding optimal IBSCs has been focused on semiconductor-dopant systems that naturally exhibit an IB [13–15], quantum dot solar cells (QDSCs) [16–20] and highly mismatched alloys (HMAs) [11, 21, 22]. In QDSCs, the confined states of a periodic array of quantum dots (QDs) lead to the formation an IB, whereas in HMAs the IB appears as a consequence of a band anti-crossing mechanism due to the localized orbitals of an isovalent dopant that perturb the CB states segregating a band from these states. Several semiconductors doped with transition metals have been proposed as good candidates for IBSCs [23–26]. Depending on the nature of the semiconductor symmetry, transition metals could introduce their *d* orbitals in the band gap, allowing the formation of an isolated IB when their concentration is sufficiently high. Since the pioneering work of Wahnón and Tablero [8], numerous theoretical studies based on density functional theory (DFT) have proposed candidates to realize IB materials: Ti-doped GaAs [8, 27] and GaP [28]; Ti- [15, 29–31], N- [32], and Au- [33] doped Silicon; Ti- [34], Cr- [35], and Sn- [36] doped $CuGaS_2$; and V-doped SnS_2 [26, 37]. Recently, Seminovski *et al* [38] investigated the formation of an intermediate band in CdTe:Bi due to the formation of (Bi_i-V_{Cd}) complexes. However, later it was experimentally observed that Bi doped CdTe exhibits an amphoteric behavior and, at high concentrations, Bi occupies a Te lattice position [39]. On the other hand, the QD approach was applied for the first time by Luque *et al* [40]. They investigated the operation of IBSC prototypes fabricated from InAs quantum dots and have shown that the quasi-Fermi levels of the conduction and intermediate bands are well separated, supporting the fundamental theory underlying the operation of the IBSC. Later, Blokhing and co-workers [41] observed efficiencies of over 18% with ∼1% gain in the short-circuit current density in a AlGaAs/GaAs single-junction cell; Ahsan *et al* [22] measured a two-photon excitation in an intermediate-band solar cell based on GaNAs; and more recently, López *et al* [42] fabricated IBSC prototypes based on InGaAs/$Al_{0.3}Ga_{0.7}As$ and reported, for the first time at room temperature, a sub-bandgap photocurrent generated by two optical transitions and the generation of an open-circuit voltage above the photon energy absorption threshold. In addition, several groups have investigated solar cells based on highly mismatched alloys. Yu *et al* [43, 44] were the first to produce an IB material based on HMAs. Wang and co-workers [11] demonstrated a ZnTe:O-based solar cell with an overall increase of 50% in power conversion efficiency when compared with a reference cell without an IB. Later, López *et al* [21] developed an IB solar cell based on GaN_xAs_{1-x}, which exhibits an open-circuit voltage of 0.92 V at room temperature, far exceeding the open-circuit voltage of 0.42 V of the reference cell.

Despite the fact that the IB scheme has been demonstrated in several systems, to the best of our knowledge high efficiency IBSCs have not yet been produced. In the present work, we show that Sn-doped CdTe is a suitable candidate for the development of full-spectrum solar cells. Motivated by its promising role in cost-effective thin-film photovoltaics [45–47] and a breakthrough in the open-circuit voltage reported early this year [48], we investigated CdTe as host semiconductor for IB photovoltaic applications. Based on the state-of-the-art DFT + *GW* formalism [49, 50], we investigated the formation energies, charge transition levels and quasiparticle defect states of several tin-related impurities in CdTe. Our results indicate that Sn occupying a Cd site in CdTe introduces an isolated IB near the midgap. Moreover, the optical spectrum obtained from the solution of the Bethe–Salpeter equation shows that this band allows the absorption of sub-bandgap photons, suggesting CdTe:Sn as a promising candidate for high-efficiency IBSCs.

2. Methods

2.1. Computational methods

We apply plane-wave supercell density functional theory calculations using the Quantum-ESPRESSO package [51]. All calculations used a plane-wave basis set with a 36 Ry cutoff and a 200 Ry cutoff to represent the charge density. We applied the generalized gradient approximation functional of Perdew, Burke, and Ernzerhof (PBE) [52] to account for the exchange-correlation effects. Electron–ion interactions were described by GBRV ultrasoft pseudopotentials [53] The defect calculations were performed using large 512-atom supercells that allow us to sample the Brillouin zone at the Γ point only. All the atoms were fully relaxed until the forces on every atom were less than 0.025 eV $Å^{-1}$.

The quasiparticle energies were calculated within the many-body G_0W_0 approximation to the electron self-energy using the WEST code [54, 55]. We used 200 projective dielectric eigenpotential basis vectors to represent the dielectric matrix and 30 Lanczos steps for evaluating the irreducible polarizability. Optimized norm-conserving Vanderbilt pseudopotentials (ONCV) [56] with 20 and 16 valence electrons for Cd and Te atoms, respectively, and a plane-wave energy cutoff of 70 Ry, were employed. For the absolute position of the VBM we used $\Delta E_{\mathrm{VBM}} = -0.74$ eV, as obtained in [57] employing the *GW*Γ approximation. Our calculated quasiparticle band gap for bulk CdTe is 1.56 eV, in excellent agreement with the experimental band gap of 1.5 eV measured at room temperature, as well as with previous calculations [58]. Moreover, the optical properties of the defects and host semiconductor are addressed, including the electron-hole interaction in the excited state by solving the Bethe–Salpeter equation (BSE) [59]. The calculations were done using the ABINIT code [60, 61]. We considered only the resonant part of the Bethe–Salpeter Hamiltonian, i.e. the Tamm–Dancoff approximation [62].

2.2. Formation energies and chemical potentials

The formation energy of a defect in the charge state q and arbitrary ionic configuration is expressed as [50, 63]

$$E_q^f[\mathbf{R}] = E_q[\mathbf{R}] - E_{\mathrm{ref}} + qE_{\mathrm{F}}, \qquad (1)$$

$$E_{\rm ref} \equiv E_{\rm bulk}^{\rm CdTe} + \sum_i n_i(\Delta\mu_i + \mu_i^{\rm ref}), \tag{2}$$

where $E_q[\mathbf{R}]$ is the total energy of the system in the charge state q and ionic configuration $\mathbf{R}$, $E_{\rm ref}$ is the energy of a reference system, and n_i is the number of atoms of species i. The integer n_i takes a positive (negative) value when the species i is added (removed) from the supercell. $\Delta\mu_i$ is a relative chemical potential for the ith atomic species referenced to $\mu_i^{\rm ref}$, which is a reference energy for the elemental bulk form. The conventional reference state for each chemical element is the phase of that element at standard conditions, i.e. the solid bulk phases for Cd, Te, and Sn. We neglected the effects of temperature and pressure, thus the reference energies were directly obtained from DFT total energies. To obtain the CdTe phase under a certain chemical environment, the chemical potentials satisfy the equation

$$\Delta\mu_{\rm Cd} + \Delta\mu_{\rm Te} = E^f[{\rm CdTe}], \tag{3}$$

where E^f[CdTe] is the formation energy of CdTe, which is calculated to be −0.91 eV, in excellent agreement with the experimental value of −0.96 eV [64]. To avoid the formation of secondary phases of Sn with the host atoms, the chemical potentials should also satisfy

$$\Delta\mu_{\rm Sn} + \Delta\mu_{\rm Te} \leqslant E^f[{\rm SnTe}], \tag{4}$$

where E^f[SnTe] is the formation energy of SnTe, which we found to be −0.59 eV, in good agreement with the experimental value of −0.63 eV [64]. The chemical potential of tin is restricted by $\Delta\mu_{\rm Sn} \leqslant \min(0, E^f[{\rm SnTe}] - \Delta\mu_{\rm Te})$.

In the Te-rich condition $\Delta\mu_{\rm Te} = 0$ and $\Delta\mu_{\rm Cd} = -0.91$ eV, then

$$\Delta\mu_{\rm Sn}^{\rm Te-rich} \leqslant -0.59{\rm eV}. \tag{5}$$

In the Cd-rich condition $\Delta\mu_{\rm Te} = -0.91$ eV and $\Delta\mu_{\rm Cd} = 0$, then

$$\Delta\mu_{\rm Sn}^{\rm Cd-rich} \leqslant 0{\rm eV}. \tag{6}$$

2.3. DFT + *GW* formalism

The most widespread model of electronic structure calculations for point defects in semiconductors is based on the density-functional theory. However, DFT suffers from the self-interaction error [65] and from the absence of the derivative discontinuity of the exchange-correlation potential [66], which lead to a number of systematic errors such as the underestimation of the band gap of semiconductors and insulators. Moreover, when the self-interaction error is properly canceled, the ground state total energy E(N) should be linear in the electron number N [67, 68]. Otherwise, approximate functionals give rise to convex or concave behavior, overstabilizing either the delocalized or the localized electron density, respectively [69].

Hybrid functionals that mix a fraction of nonlocal Fock exchange with local density approximation (LDA) or generalized gradient (GGA) functionals have demonstrated to correct the band gap problem to a large extent. Moreover, it has been shown that they give an excellent description of the electronic structure for both the perfect crystal and defect states, provided the defect states are more host than impurity related [70]. However, the defect systems are composite systems in which the defect states and the host states may experience different screening, and thus one has to be cautious in choosing the mixing and screening parameters [71, 72].

The DFT + *GW* approach [49, 50, 73] combines DFT with the many-body Green's-function formalism. According to equation (1), the formation energy of a defect in the charge state $q-1$ is given by

$$E_{q-1}^f[\mathbf{R}_{q-1}] = E_{q-1}[\mathbf{R}_{q-1}] - E_{\rm ref} + (q-1)E_{\rm F}. \tag{7}$$

By adding and substracting first $E_{q-1}[\mathbf{R}_q]$ and then $E_q[\mathbf{R}_q]$, we have

$$\begin{aligned} E_{q-1}^f[\mathbf{R}_{q-1}] &= \left\{E_{q-1}[\mathbf{R}_q] - E_q[\mathbf{R}_q]\right\} \\ &\quad + \left\{E_{q-1}[\mathbf{R}_{q-1}] - E_{q-1}[\mathbf{R}_q]\right\} \\ &\quad + E_q^f[\mathbf{R}_q] - E_{\rm F} \\ &\equiv E_{\rm QP} + E_{\rm relax} + E_q^f[\mathbf{R}_q] - E_{\rm F}, \end{aligned} \tag{8}$$

where $\mathbf{R}_q$ corresponds to the minimum energy configuration for the charge state q.

Similarly, adding first $E_{q+1}[\mathbf{R}_q]$ and then substracting $E_q[\mathbf{R}_q]$ to equation (7), we have

$$\begin{aligned} E_{q+1}^f[\mathbf{R}_{q+1}] &= \left\{E_{q+1}[\mathbf{R}_q] - E_q[\mathbf{R}_q]\right\} \\ &\quad + \left\{E_{q+1}[\mathbf{R}_{q+1}] - E_{q+1}[\mathbf{R}_q]\right\} \\ &\quad + E_q^f[\mathbf{R}_q] + E_{\rm F} \\ &\equiv E_{\rm QP} + E_{\rm relax} + E_q^f[\mathbf{R}_q] + E_{\rm F}. \end{aligned} \tag{9}$$

The first term in equations (8) and (9) is a quasiparticle energy ($E_{\rm QP}$), which corresponds to the addition or removal of a single electron to a reference system. This quantity is not accurately described within DFT, but it may be evaluated using the *GW* approximation [74, 75]. Using Kohn–Sham wave functions $\psi_{n,k}^{\rm KS}$ and energies $\epsilon_{n,k}^{\rm KS}$ as a zeroth-order approximation in the construction of G and W (known as G_0W_0 approximation), we calculate the quasiparticle energies $E_{n,k}^{\rm QP}$ within a first-order perturbation theory approximation as

$$E_{n,k}^{\rm QP} = \epsilon_{n,k}^{\rm KS} + \left\langle \psi_{n,k}^{\rm KS} | \Sigma(E_{n,k}^{\rm QP}) - V_{\rm xc} | \psi_{n,k}^{\rm KS} \right\rangle, \tag{10}$$

which comes from replacing the Kohn–Sham exchange-correlation potential $V_{\rm xc}$ with the self-energy operator Σ. When the reference state is an open-shell system, we use spin-polarized DFT calculations as mean-field starting points for G_0W_0. Due to the high computational demands of the calculations, we employed a cubic 64-atom supercell to evaluate the quasiparticle corrections to the Kohn–Sham eigenvalues at the Γ point only. Then, these corrections were applied to the KS eigenvalues of 512-atom supercells to obtain the quasiparticle energies with respect to the average electrostatic potential of pristine CdTe. We note that the quasiparticle corrections are

Table 1. Defect formation energies used as reference for the DFT + *GW* scheme. The Fermi energy is set equal to the valence band maximum (all values are given in eV).

Reference system	E^f (Te-rich)	E^f (Cd-rich)
$(Sn_{Cd})^{+2}$	−1.43	−1.11
$(Sn_{Cd} - V_{Cd})^0$	1.04	2.27
$(Sn_{Te})^0$	3.32	1.82
$(Sn_i)^{+2}$	−0.61	−1.20

largely invariant with respect to the supercell size [35, 50, 76] and we consider the finite-size effects at DFT level.

The second term in equations (8) and (9) corresponds to the ionic relaxation energy (E_{relax}) of the system to its new minimum-energy configuration after the addition or removal of a single electron. This term can be calculated at the DFT level since we avoid the computation of energy differences between systems with different electronic configurations. In this work, we calculate the relaxation energies using 512-atom supercells.

2.4. Comparison with the generalized gradient approximation (GGA)

According to our results, the electronic structure of the intermediate-band material is qualitatively well described at the DFT-PBE level despite the well-known problem of band gap underestimation in GGA. The impurity band appears near the middle of the band gap, as in the G_0W_0 approximation. Interestingly, this intermediate-band (which is mainly derived from Sn 5s states) does not track the shift of the valence band maximum or the conduction band minimum, indicating that the quasiparticle corrections depend on the character of the electronic states, thus there is no simple 'scissor rule' to obtain the quasiparticle band structure.

2.5. Reference energy for the DFT + *GW* scheme

The DFT + *GW* formalism relies on the quality of at least one formation energy calculated within the DFT. This energy is used as a reference to obtain the formation energies for different charge states by using equations (8) and (9). A key observation is that when all the valence bands are full and all the conduction bands are empty, the self-interaction error (which artificially raises the VBM) will mostly cancel in the first difference of equation (1). For example, starting from $q = +2$, the formation energies for (Sn_{Cd}) in the charge states (0), (−1), and (−2) can be computed by the successive application of equation (8).

The formation energies used as a reference in this work are shown in table 1.

3. Results and discussion

3.1. Defect formation energies of Sn impurities

The formation energy provides information on the stability of a given defect or impurity and determines its concentration through a Boltzmann relation [77]:

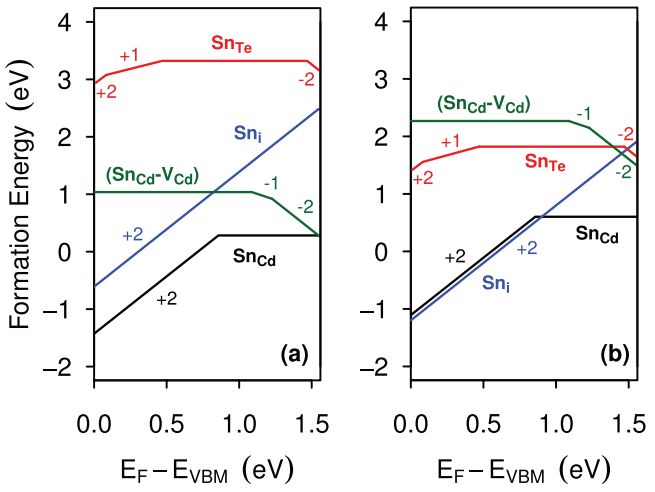

Figure 1. Calculated formation energies of Sn impurities in various charge states as a function of the Fermi level inside the band gap corresponding to (a) Te-rich conditions and (b) Cd-rich conditions. The numbers next to the lines indicate the charge state.

$$C = N_s e^{-E_q^f/kT}, \tag{11}$$

where N_s is the number of possible defect sites, k is Boltzmann's constant, and T is the temperature. To determine the energetically most favorable lattice site for Sn in CdTe, the formation energy of the tin atom at each charge state was calculated at the interstitial and at the substitutional Cd and Te sublattices. In addition, we studied the ($Sn_{Cd} - V_{Cd}$) complex, since it has been established that the dominant intrinsic defect in CdTe is the Cd vacancy (V_{Cd}) [78–80], which is believed to be associated with foreign impurities as well as with native defects.

The formation energies of Sn at different lattice sites are shown in figure 1 as a function of Fermi energy, for Te-rich and Cd-rich growth conditions. In the Te-rich growth condition, we observe that the most stable is the substitutional site (Sn_{Cd}), where Sn acts as deep double donor. It has a relatively low formation energy, exhibiting a (+2/0) charge transition level at VBM + 0.85 eV. This result is in good agreement with the experimental measurements [81, 82]. As shown in figure 2(b), an isolated IB is introduced near the middle of the band gap. This energy level is mainly dominated by the Sn 5s states (figure 3(b)) and is discussed in the next section.

According to our results, the interstitial tin (Sn_i) is tetrahedrally coordinated by Cd atoms and is stable only in the double positive charge state. Its electronic structure has no levels in the band gap, which is consistent with the fact that all bonds are satisfied. In the Cd-rich limit, its formation energy is lower than that for (Sn_{Cd}) when the Fermi level is close to the VBM. On the other hand, under n-type conditions (Sn_{Cd}) in the neutral charge state might be favored.

In addition, it is widely accepted that Te-rich CdTe films have p-type conductivity and a high concentration of Cd vacancies [83, 84]. As (V_{Cd}) is a relatively shallow double acceptor, it should tend to be in the double negative charge state. Therefore, in order to preserve the crystal electroneutrality, the formation of ($Sn_{Cd} - V_{Cd}$) complexes may be favored [85]. Our results show that this complex is a deep acceptor with electron trapping levels calculated at VBM + 1.10 eV (0/−)

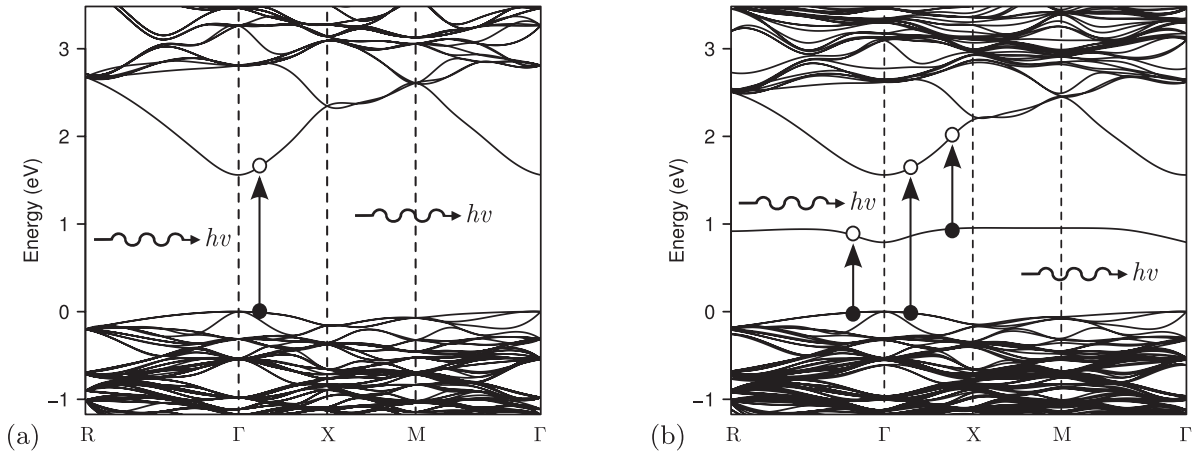

Figure 2. Electronic band structures of (a) perfect CdTe, and (b) CdTe containing a single (Sn_{Cd}) impurity, calculated in a 216-atom supercell. The vertical arrows represent photon absorptions.

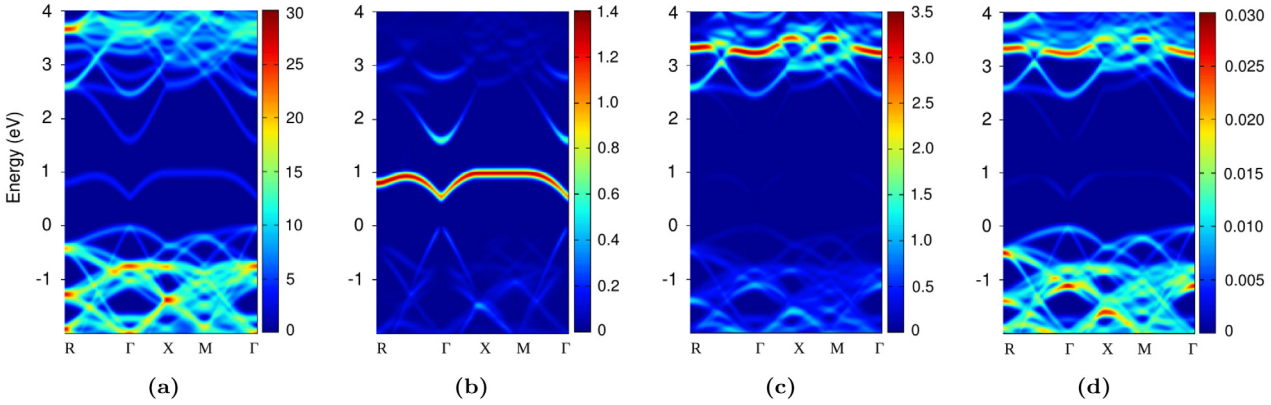

Figure 3. (a) **k**-resolved total density of states of CdTe containing an isolated (Sn_{Cd}) impurity, and **k**-resolved projected density of states corresponding to (b) Sn 5s (c) Sn 5p, and (d) Sn 4d atomic orbitals (in states/eV), calculated in a 64-atom supercell. (a) Total. (b) Sn 5s. (c) Sn 5p. (d) Sn 4d.

and VBM + 1.24 eV (−/−2), respectively. Its electronic structure exhibits a deep energy level in the band gap, mainly derived from the contribution of Sn 5s states similar to (Sn_{Cd}).

Next, we turn to the substitutional tin (Sn_{Te}). According to the work of Lany *et al* [86], at T_d symmetry the tellurium vacancy introduces a singlet a_1 state and a triplet t_2 state. In the neutral charge state, the a_1 state is fully occupied by two electrons and the t_2 state is empty, thus no Jahn–Teller effect is expected [87]. However, when a Sn atom occupies the vacancy site its four valence electrons will partially fill into the t_2 state, leaving the system in an electronic degenerate state. In this case, the system would be unstable with respect to symmetry-lowering distortions that minimize the total electronic energy. Our results show that a distortion from T_d to C_{3v} removes the degeneracy stabilizing the system. These localized energy levels are likely to act as harmful recombination centers. Fortunately, the formation energy of (Sn_{Te}) is high in both Te-rich and Cd-rich grown conditions, so it is unlikely to form at a substantial concentration. It is worth noting that our results for (Sn_{Te}) strongly differ from [88], in which a small 16-atom supercell was employed and the Jahn–Teller distortion was not considered.

Finally, our results suggest that (Sn_{Cd}) and (Sn_i) might tend to push the Fermi energy to higher values in the band gap, which is consistent with the *n*-type conductivity experimentally observed in CdTe:Sn [89]. In addition, recent results have indicated that the lifetime and hole density are simultaneously increased by annealing the samples in a Cd overpressure [48]. Moreover, a Cd-rich environment would favor Sn incorporation via interstitial or kick-out [90] diffusion mechanisms, as the formation energy of (Sn_i) is lowered with respect to the Te-rich limit.

3.2. Suppressing non-radiative recombination

It is known that the impurities that introduce localized states in the band gap increase non-radiative Shockley–Read–Hall recombination [91, 92]. Moreover, when the ground state energy of those defects is well separated from the band-edges (by a large energy of the order of tenths of an electronvolt), it has been proposed that carrier capture by such centers should be accompanied by the simultaneous emission of many phonons (lattice-relaxation multiphonon emission) [93].

In semiconductors, electrons in the conduction and valence bands are characterized by delocalized Bloch wave functions extending across the whole crystal. In contrast, the electrons in the deep traps are well localized in the sense of Anderson [94]. Moreover, when a free electron (or hole) is captured the system becomes strongly out of equilibrium, since the charge

formerly distributed across the whole crystal is suddenly closely packed around the impurity. After carrier capture, the system can be described as a bound electron (or hole) plus a highly excited vibrational state, and there follows a relaxation process involving the release of the excess energy as lattice phonons.

On the other hand, when the impurity concentration is high (so that the Mott transition is produced) the atomic wave functions localized in different impurity atoms overlap and lose their localized character. It is often said that an impurity band is formed as the banding or 'resonance' energy between different sites becomes larger as compared to the variation of the local electric fields, due to nearby ionized acceptors and donors. In this scenario, carrier trapping does not involve a large charge movement in the space, and thus trap-assisted non-radiative recombination can be suppressed. Experimental confirmation of this fact has been recently reported in [23] and [95].

Moreover, delocalization by means of a Mott transition is expected for concentrations above $5.9 \times 10^{19}\,\mathrm{cm}^{-3}$ at 300 K. However, high impurity concentrations could cause Sn starts to form aggregates or the formation of a $Cd_{1-x}TeSn_x$ ternary alloy. Thus, for good quality samples, a moderate doping level just above the Mott transition would be recommended.

3.3. Isolated intermediate-band

As was noted in the introduction, several semiconductors doped with transition metals have been proposed as good candidates for IBSCs. However, metal-dopant 3d states that form the IB are rather localized, leading to low sub-bandgap absorption coefficients. Thus, transition metal doping may not be the best approach to build high-efficiency IBSCs [36]. In the case of CdTe:Sn, an isolated intermediate band is formed when a Sn impurity occupies a Cd vacancy site. Further insights can be gained from the **k**-resolved projected density of states shown in figure 3. It reveals that this impurity band is derived mainly from Sn 5s states, which are also hybridized with the Te 5p orbitals that largely contribute to the extended states of the conduction band minimum. This s-derived IB allows three direct band gap transitions (VB → IB, IB → CB, VB → CB), as depicted in figure 2(b).

3.4. Partial filling of the intermediate-band

According to the IB scheme, the intermediate band should be isolated and partially filled in order to allow three direct band gap transitions. Moreover, the occupancy of the IB may vary with light intensity, cell voltage, density of IB-states, thickness of the material, concentration of native defects and its position in the band gap of the host semiconductor. From the theoretical point of view, predicting the occupancy of an IB in thermodynamic equilibrium is actually a very challenging task. For example, first-principles calculations predict the existence of a partially filled IB in V-doped In_2S_3 [96, 97]. However, Hall measurements reveal an excess *n*-type carriers due to intrinsic donors in In_2S_3 and $V_xIn_{(2-x)}S_3$, thereby biasing the Fermi energy toward the conduction bands. As a consequence, the IB is largely filled and exhibits photocurrent response only to illumination wavelengths with an energy equal to or greater than the host semiconductor band gap [98].

In the case of CdTe, most polycrystalline films require high growth temperatures (450–600 °C) resulting in Te excess (due to the loss of Cd during the growth process) and *p*-type conductivity [99]. According to figure 1, Sn atoms would tend to transfer their electrons to uncompensated acceptors such as (V_{Cd}). If the concentration of Sn donors exceeds the concentration of shallow acceptors, (Sn_{Cd}) might tend to be in the neutral charge state, pinning the Fermi energy at (+2/0) and thereby leading to *n*-type conductivity. More importantly, the Fermi energy is most likely to be pinned over the IB that will form when the concentration of Sn impurities is increased above the insulator-to-metal transition described in section 3.2. It is worth mentioning that (Sn_{Cd}) could also act as an effective electron trap for concentrations below the Mott transition, explaining the ∼0.7-0.8 eV C-band deep-level recombination observed in photoluminescence measurements [100].

Another way to achieve the partial filling of the IB was proposed by Strandberg and Reenaas [101]. They have shown that partial filling can be also achieved by optical pumping or photofilling when the cell is exposed to concentrated light. Moreover, a photofilled IBSC can give efficiencies comparable to those of a prefilled IBSC.

3.5. Optical properties

In order to investigate the optical behavior of Sn-doped CdTe, we calculate its absorption spectrum from first principles. We focus on a single substitutional tin impurity occupying a Cd site (Sn_{Cd}). The electron-hole interaction is included on the level of the BSE, which yields both bound and unbound, i.e. resonant excitations. The defect calculation was performed in a $3 \times 3 \times 2$ supercell of CdTe containing a single impurity, which corresponds to a concentration of Sn atoms of 2.8%. The BSE Hamiltonian was constructed including four valence bands and eight conduction bands in the electron-hole basis set. We used a $3 \times 3 \times 4$ **k**-grid shifted along the (0.11, 0.12, 0.13) direction, which is interpolated to a much finer $6 \times 6 \times 8$ grid by using the scheme proposed by Gillet *et al* [102]. Our tests show that these parameters are sufficient to obtain a well-converged BSE spectrum within 0.1 eV. It is worth mentioning that a considerable improvement in efficiency was obtained by using the memory-efficient technique recently proposed in [102].

The optical absorption spectrum is described by the imaginary part of the macroscopic dielectric function $\mathrm{Im}\{\epsilon_M(\omega)\}$, as shown in figure 4. As expected, in the case of undoped CdTe, no absorption is observed in the energy region below the band gap edge. After doping, the absorption increases significantly in the band gap region, due to the isolated IB states introduced by the dopant 5s orbitals. The absorption peak at about 0.8 eV is due to transitions between the intermediate and conduction bands, suggesting that the IB allows optical transitions for sub-bandgap photons. Moreover, the contribution due to the transitions between the valence bands and the intermediate band starts at about 0.9 eV. Our results are in agreement with the optical transmittance spectra of CdTe and CdTe:Sn reported

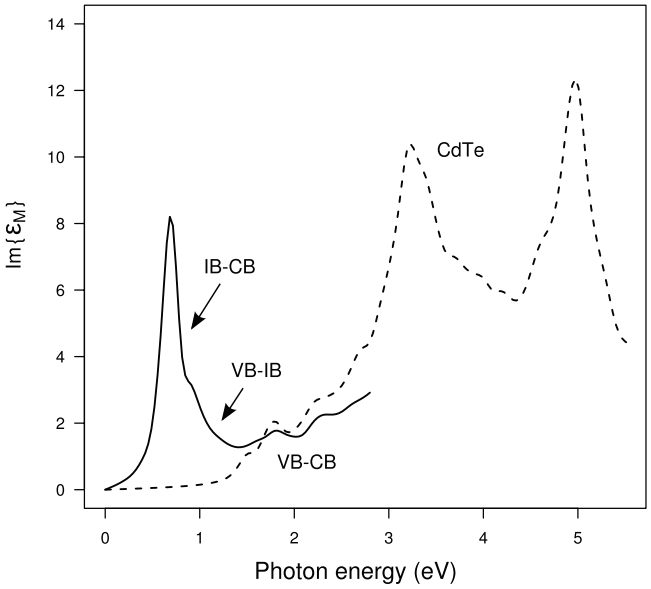

Figure 4. Comparison of the bulk CdTe optical spectrum (dashed line) with the spectrum computed in a $3 \times 3 \times 2$ supercell of CdTe with a single Sn impurity occupying a Cd site (solid line).

in [89] (in this reference, the sample CdTe:Sn1 corresponds to a Sn concentration of 3.59%). In our opinion this is a clear indication of the IB existence. Unfortunately, the maximum wavelength explored in [89] (1100 nm) is too short to verify the strong absorption peak induced by IB $\rightarrow$ CB transitions.

4. Conclusions

In summary, we have investigated the possibility of increasing the photocurrent in CdTe photovoltaic material via two-step photoexcitation by using an intermediate-band as a stepping stone. We have investigated the formation energies, charge transition levels and quasiparticle defect states of several tin-related impurities in CdTe, within the DFT + *GW* theoretical approach. Our calculations indicate that Sn occupying a Cd site in CdTe induces a (+2/0) transition level at VBM + 0.85 eV. The electronic properties of (Sn_{Cd}) reveal the existence of an isolated impurity band mainly derived from Sn 5s states. Moreover, it exhibits the lowest formation energy under Te-rich conditions, suggesting a stable impurity.

In addition, we investigated the optical properties of Sn-doped CdTe based on the solution of the Bethe–Salpeter equation. The optical spectrum shows a strong absorption at photon energies near 0.8 eV, which are attributed to transitions between the IB and the CB. Furthermore, our results indicate that electrons are also excited from the VB to the IB and from the VB to the CB. Therefore, we propose Sn-doped CdTe as a good candidate for highly efficient intermediate-band solar cells, which could potentially overcome the Shockley–Queisser limit.

Acknowledgments

This work was supported by the Fondo Nacional de Desarrollo Científico y Tecnológico (FONDECYT, Chile) under Grant No. 1130437, and by CONACYT-SENER SUSTENTABILIDAD ENERGETICA (México) under project CeMIE-Sol PY-207450/25 and PY-207450/26. Powered@NLHPC: This research was partially supported by the supercomputing infrastructure of the NLHPC (ECM-02).

References

[1] Shockley W and Queisser H J 1961 *J. Appl. Phys.* **32** 510
[2] King R R *et al* 2012 *Prog. Photovolt., Res. Appl.* **20** 801–15
[3] Green M A, Emery K, Hishikawa Y, Warta W and Dunlop E D 2015 *Prog. Photovolt., Res. Appl.* **23** 805–12
[4] Würfel P 1997 *Sol. Energy Mater. Sol. Cells* **46** 43–52
[5] Le Bris A and Guillemoles J F 2010 *Appl. Phys. Lett.* **97** 113506
[6] Wolf M 1960 *Proc. IRE* **48** 1246–63
[7] Luque A and Martí A 1997 *Phys. Rev. Lett.* **78** 5014
[8] Wahnón P and Tablero C 2002 *Phys. Rev.* B **65** 165115
[9] Luque A, Martí A and Stanley C 2012 *Nat. Photon.* **6** 146
[10] Mlinar V 2013 *Nanotechnology* **24** 042001
[11] Wang W, Lin A and Phillips J 2009 *Appl. Phys. Lett.* **95** 011103
[12] Martí A and Araujo G 1996 *Sol. Energy Mater. Sol. Cells.* **43** 203
[13] Palacios P, Wannón P, Pizzinato S and Conesa J 2006 *J. Chem. Phys.* **124** 14711
[14] Palacios P, Aguilera I, Sánchez K, Conesa J and Wannón P 2008 *Phys. Rev. Lett.* **101** 046403
[15] Sánchez K, Aguilera I, Palacios P and Wannón P 2008 *Phys. Rev.* B **79** 165203
[16] Martí A, Cuadra L and Luque A 2000 Quantum dot intermediate band solar cell *Proc. 28th IEEE Photovoltaics Specialists Conf.* (IEEE) pp 904–43
[17] Luque A, Martí A, López N, Antolín E and Cánovas E 2005 *Appl. Phys. Lett.* **87** 083505
[18] Oshima R, Takata A and Okada Y 2008 *Appl. Phys. Lett.* **93** 083111
[19] Shoji Y, Akimoto K and Okada Y 2013 *J. Phys. D: Appl. Phys.* **46** 024002
[20] Sogabe T *et al* 2014 *Sci. Rep.* **4** 4792
[21] López N, Reichertz L, Yu K, Campman K and Walukiewicz W 2011 *Phys. Rev. Lett.* **106** 028701
[22] Ahsan N *et al* 2012 *Appl. Phys. Lett.* **100** 172111
[23] Persans P D, Berry N E, Recht D, Hutchinson D, Peterson H, Clark J, Charnvanichborikarn S, Williams J S, DiFranzo A, Aziz M J and Warrender J M 2012 *Appl. Phys. Lett.* **101** 111105
[24] Castán H, Pérez E, García H, Dueñas S, Bailón L, Olea J, Pastor D, García-Hemme E, Irigoyen M and González-Díaz G 2013 *J. Appl. Phys.* **113** 024104
[25] Strandberg R and Aguilera I 2012 *Sol. Energy Mater. Sol. Cells* **98** 88–93
[26] Seminovski Y, Palacios P and Wahnón P 2014 *J. Phys.: Condens. Matter* **26** 395501
[27] Wahnón P, Palacios P, Fernández J J and Tablero C 2005 *J. Mater. Sci.* **40** 1383–6
[28] Tablero C and Wahnón P 2003 *Appl. Phys. Lett.* **82** 151
[29] Olea J, González-Díaz G, Pastor D and Mártil I 2009 *J. Phys. D: Appl. Phys.* **42** 085110
[30] Pastor D, Olea J, del Prado A, García-Hemme E, García-Hernansanz R, Mártil I and González-Díaz G 2013 *J. Phys. D: Appl. Phys.* **46** 135108
[31] Olea J, López E, Antolín E, Martí A, Luque A, García-Hemme E, Pastor D, García-Hernansanz R, del Prado A and González-Díaz G 2016 *J. Phys. D: Appl. Phys.* **49** 055103

[32] Zhu Z, Shao H, Dong X, Li N, Ning B Y, Ning X J, Zhao L and Zhuang J 2015 *Sci. Rep.* **5** 10513
[33] Mailoa J P *et al* 2013 *Nat. Commun.* **5** 3011
[34] Palacios P, Sánchez K, Conesa J, Fernández J and Wahnón P 2007 *Thin Solid Films* **515** 6280–4
[35] Chen P, Qin M, Chen H, Yang C, Wang Y and Huang F 2013 *Phys. Status Solidi* a **210** 1098–102
[36] Yang C, Qin M, Wang Y, Wan D, Huang F and Lin J 2013 *Sci. Rep.* **3** 1286
[37] Wahnón P, Conesa J C, Palacios P, Lucena R, Aguilera I, Seminovski Y and Fresno F 2011 *Phys. Chem. Chem. Phys.* **13** 20401–7
[38] Seminovski Y, Palacios P and Wahnón P 2013 *Sol. Energy Mater. Sol. Cells* **114** 99–103
[39] Vigil-Galán O, Courel M, Cruz-Gandarilla F and Seuret-Jiménez D 2016 *J. Mater. Sci., Mater. Electron.* **27** 6088–95
[40] Luque A, Martí A, Stanley C, López N, Cuadra L, Zhou D, Pearson J L and McKee A 2004 *J. Appl. Phys.* **96** 903–9
[41] Blokhin S A *et al* 2009 *Semiconductors* **43** 514–8
[42] López E *et al* 2016 *Sol. Energy Mater. Sol. Cells* **149** 15–8
[43] Yu K, Walukiewicz W, Wu J, Shan W, Beeman J, Scarpulla M, Dubon O and Becla P 2003 *Phys. Rev. Lett.* **91** 246403
[44] Yu K, Walukiewicz W, Ager J III, Bour D, Farshchi R, Dubon O, Li S, Sharp I and Haller E 2006 *Appl. Phys. Lett.* **88** 092110
[45] Rejón V, Riech I and Peña J L 2013 *Sol. Energy* **95** 319–24
[46] Mahabaduge H P *et al* 2015 *Appl. Phys. Lett.* **106** 133501
[47] Gretener C, Perrenoud J, Kranz L, Cheah E, Dietrich M, Buecheler S and Tiwari A 2016 *Sol. Energy Mater. Sol. Cells* **146** 51–7
[48] Burst J M *et al* 2016 *Nat. Energy* **1** 16015
[49] Rinke P, Janotti A, Scheffler M and Van de Walle C G 2009 *Phys. Rev. Lett.* **102** 026402
[50] Flores M A, Orellana W and Menéndez-Proupin E 2016 *Phys. Rev.* B **93** 184103
[51] Giannozzi P *et al* 2009 *J. Phys.: Condens. Matter* **21** 395502
[52] Perdew J, Burke K and Ernzerhof M 1996 *Phys. Rev. Lett.* **77** 3865
[53] Garrity K, Bennett J, Rabe K and Vanderbilt D 2014 *Comput. Mater. Sci.* **81** 446
[54] Pham T A, Nguyen H V, Rocca D and Galli G 2013 *Phys. Rev.* B **87** 155148
[55] Govoni M and Galli G 2015 *J. Chem. Theory Comput.* **11** 2680–96
[56] Hamann D 2013 *Phys. Rev.* **88** 085117
[57] Grüneis A, Kresse G, Hinuma Y and Oba F 2014 *Phys. Rev. Lett.* **112** 096401
[58] Klimes J, Kaltak M and Kresse G 2014 *Phys. Rev.* B **90** 075125
[59] Rohlfing M and Louie S G 1998 *Phys. Rev. Lett.* **81** 2312–5
[60] Gonze X *et al* 2009 *Comput. Phys. Commun.* **180** 2582–615
[61] Gonze X *et al* 2016 *Comput. Phys. Commun.* **205** 106–31
[62] Benedict L X, Shirley E L and Bohn R B 1998 *Phys. Rev. Lett.* **80** 4514–7
[63] Flores M A, Orellana W and Menéndez-Proupin E 2016 *Comput. Mater. Sci.* **125** 176–82
[64] Haynes W (ed) 2014 *CRC Handbook of Chemistry and Physics* 95th edn (Boca Raton, FL: CRC Press)
[65] Perdew J P and Zunger A 1981 *Phys. Rev.* B **23** 5048–79
[66] Perdew J P, Parr R G, Levy M and Balduz J L 1982 *Phys. Rev. Lett.* **49** 1691–4
[67] Perdew J P, Ruzsinszky A, Csonka G I, Vydrov O A, Scuseria G E, Staroverov V N and Tao J 2007 *Phys. Rev.* A **76** 040501
[68] Cohen A J, Mori-Sánchez P and Yang W 2008 *Science* **321** 792–4
[69] Sai N, Barbara P F and Leung K 2011 *Phys. Rev. Lett.* **106** 226403
[70] Deák P, Aradi B, Frauenheim T, Janzén E and Gali A 2010 *Phys. Rev.* B **81** 153203
[71] Lany S and Zunger A 2010 *Phys. Rev.* B **81** 205209
[72] Bang J, Sun Y Y, Abtew T A, Samanta A, Zhang P and Zhang S B 2013 *Phys. Rev.* B **88** 035134
[73] Malashevich A, Jain M and Louie S G 2014 *Phys. Rev.* B **89** 075205
[74] Hedin L 1965 *Phys. Rev.* **139** A796
[75] Hybertsen M S and Louie S G 1985 *Phys. Rev. Lett.* **55** 1418–21
[76] Choi E A and Chang K J 2009 *Appl. Phys. Lett.* **94** 122901
[77] Van de Walle C G and Neugebauer J 2004 *J. Appl. Phys.* **95** 3851–79
[78] Figueroa J M, Sánchez-Sinencio F, Mendoza-Álvarez J G, Zelaya O, Vázquez-López C and Helman J S 1986 *J. Appl. Phys.* **60** 452–4
[79] Emanuelsson P, Omling P, Meyer B K, Wienecke M and Schenk M 1993 *Phys. Rev.* B **47** 15578–80
[80] Shepidchenko A, Sanyal B, Klintenberg M and Mirbt S 2015 *Sci. Rep.* **5** 14509
[81] Panchuk O, Savitskiy A, Fochuk P, Nykonyuk Y, Parfenyuk O, Shcherbak L, Ilashchuk M, Yatsunyk L and Feychuk P 1999 *J. Cryst. Growth* **197** 607–11
[82] Babentsov V, Franc J, Elhadidy H, Fauler A, Fiederle M and James R B 2007 *J. Mater. Res.* **11** 3249
[83] Friedman D, Olson J and Kurtz S 2011 *Handbook of Photovoltaic Science and Engineering* 2nd edn (Chichester: Wiley)
[84] de Moure-Flores F *et al* 2012 *J. Appl. Phys.* **112** 113110
[85] Grill R, Turkevych I, Franc J, Belas E, Moravec P and Höschl P 2004 *Phys. Status Solidi* c **1** 727–30
[86] Lany S, Ostheimer V, Wolf H and Wichert T 2001 *Physica* B **308–10** 958–62
[87] Menéndez-Proupin E and Orellana W 2015 *Phys. Status Solidi* b **252** 2649–56
[88] Jaffe J 2006 *J. Appl. Phys.* **99** 033704
[89] Quiñones-Galván J G, Guillén-Cervantes A, Campos-González E, Santos-Cruz J, Mayén-Hernández S A, Olvera M D L L, Zelaya-Angel O, Contreras-Puente G and de Moure-Flores F 2016 *J. Laser Appl.* **28** 032012
[90] Gösele U, Frank W and Seeger A 1980 *Appl. Phys.* **23** 361–8
[91] Shockley W and Read W 1952 *Phys. Rev.* **87** 835
[92] Hall R 1952 *Phys. Rev.* **87** 387
[93] Lang D V and Henry C H 1975 *Phys. Rev. Lett.* **35** 1525–8
[94] Anderson P W 1958 *Phys. Rev.* **109** 1492–505
[95] Antolín E, Martí A, Olea J, Pastor D, González-Díaz G, Mártil I and Luque A 2009 *Appl. Phys. Lett.* **94** 042115
[96] Lucena R, Aguilera I, Palacios P, Wahnón P and Conesa J C 2008 *Chem. Mater.* **20** 5125–7
[97] Lucena R, Conesa J, Aguilera I, Palacios P and Wahnón P 2014 *J. Mater. Chem.* A **2** 8236
[98] McCarthy R F, Weimer M S, Haasch R T, Schaller R D, Hock A S and Martinson A B 2016 *Chem. Mater.* **28** 2033–40
[99] de Moure-Flores F *et al* 2014 *J. Cryst. Growth* **386** 27–31
[100] Fiederle M, Babentsov V, Franc J, Fauler A and Konrath J P 2003 *Cryst. Res. Technol.* **38** 588–97
[101] Strandberg R and Reenaas T 2009 *J. Appl. Phys.* **105** 124512
[102] Gillet Y, Giantomassi M and Gonze X 2016 *Comput. Phys. Commun.* **203** 83–93